Vibrational resonance in nonlinear maps

S. Rajasekar*

School of Physics, Bharathidasan University,

Tiruchirappalli 620 024, Tamilnadu, India

Javier Used,† Alexandre Wagemakers,‡ and M.A.F. Sanjuan§

Departamento de Física, Universidad Rey Juan Carlos,

Tulipán s/n, 28933 Móstoles, Madrid, Spain

Abstract

We investigate vibrational resonance in two different nonlinear maps driven by a biharmonic force: the Bellows and the Rulkov map. These two maps possess dynamical features of particular interest for the study of these phenomena. In both maps, the resonance occurs at the low-frequency of the biharmonic signal as the amplitude of the high-frequency is varied. We also consider a chain of unidirectionally coupled maps with the forcing signal applied to the first unit. In this case, a signal propagation with several interesting features above a critical value of the coupling strength is found, while the response amplitude of the ith unit is greater than the first one. This response evolves in a sigmoidal fashion with the system number i, meaning that at some point the amplitudes saturate. The unidirectional coupling acts as a low-pass filter for distant units. Moreover, the analysis of the mean residence time of the trajectory in a given region of the phase space unveils a multiresonance mechanism in the coupled map system. These results point at the relevance of the discrete-time models for the study of resonance phenomena, since analyses and simulations are much easier than for continuous-time models.

PACS numbers: 05.45.-a, 05.90.+m, 46.40.Ff, 87.19.II

Keywords: Vibrational resonance, biharmonic force, Bellows map, Rulkov map, signal propagation.

*Electronic address: rajasekar@cnld.bdu.ac.in

†Electronic address: javier.used@urjc.es

‡Electronic address: alexandre.wagemakers@urjc.es

§Electronic address: miguel.sanjuan@urjc.es

I. INTRODUCTION

The presence of noise in dynamical systems is often considered as a nuisance source that degrades the performance and perturbs their behavior. However, in certain nonlinear systems driven by a low-amplitude periodic force, the response at the frequency of the driving force can be enhanced by an optimal noise. This noise-induced phenomenon is termed as stochastic resonance [1, 2]. In recent years, another type of resonance reported first by Landa and McClintock [3], called vibrational resonance (VR) has received a considerable attention. They have shown that in a bistable system driven by both a low and a high-frequency force, the response amplitude at the low-frequency increases, reaches a maximum and then decreases as the amplitude of the high-frequency force is varied. Later, Gitterman [4] and Blekhman and Landa [5] developed the theoretical aspects of the VR. So far, this phenomenon has been thoroughly studied in a large class of dynamical systems such as a noise induced structure [6], the FitzHugh–Nagumo equation [7], coupled oscillators [8], a multistable system [9], a monostable system [10], small-world networks [11, 12], spatially periodic potential system [13, 14], time-delayed systems [15, 16] and many more.

So far, VR has been studied in continuous-time dynamical systems described by nonlinear ordinary differential equations. We want to show in this paper that this phenomenon also appears in simple and flexible models as can be the discrete-time dynamical systems, also termed as maps. There are several specific advantages of using a map as a reference model system in the investigation of fundamental features of a phenomenon. For example, solving numerically a large array of coupled dynamical systems is a time-consuming simulation, while a system of m coupled maps requires relatively few computational resources. Algorithms of statistical measures are often relatively much easier for maps than for the systems described by ordinary differential equations. Furthermore, there are many simple maps displaying monostable, bistable, multistable and excitable behaviours making them paradigmatic models for the study of continuous-time dynamical systems with similar characteristics. Despite its apparent simplicity, these maps can reproduce faithfully the dynamics of some physical and biological systems from which they derive [17–19] and can be used for an easier understanding of the phenomenon of VR in these systems.

This is precisely what motivates us to consider here the Bellows map with bistable states and the Rulkov map capable of exhibiting excitable and bursting dynamics. We numerically

analyze the occurrence of VR in a single and a coupled version of these maps driven by a biharmonic force with two frequencies ω and Ω, being $\Omega \gg \omega$. Similarities and differences arise in the mechanism of VR in these two different kinds of maps. While studying the coupled maps, we only consider the excitation of the first map by the biharmonic signal, while the coupling is linear and unidirectional. There is no coupling term in the first map. In the two types of coupled arrays, that is coupled Bellows maps and coupled Rulkov maps, above a critical value of the coupling strength, an undamped signal propagation takes place with a few interesting features. We note that in coupled systems, particularly, in biological network systems, an undamped signal propagation is essential for information transmission as for example the signal propagation among neurons. Multiple VR occurs in all the coupled subsystems, even though the first system shows only a single resonance. As we look at units separated by i links from the first unit, the response amplitude at the lower frequency ω increases and reaches a constant value as i increases, while the amplitude at the frequency Ω decreases with i.

II. VIBRATIONAL RESONANCE IN SINGLE MAPS

First we consider the Bellows map [20–22] represented by the following equation:

$$x_{n+1} = f(x_n) = \frac{r x_n}{1 + x_n^b}. \tag{1}$$

This simple one-dimensional map has different behaviors depending on the parameter r. This map models the evolution of the population density of an organism, where r is a parameter related to an environmental factor. Equation (1) has only one fixed point $x^* = 0$ for $b = 2$ and for $0 < r \leq 1$. For $r > 1$, it has three fixed points with $x_0^* = 0$ being unstable, while $x_\pm^* = \pm\sqrt{r-1}$ being stable. That is, the Bellows map has a monostable state for $0 < r \leq 1$ and a bistable state for $r > 1$.

The other map in consideration is the Rulkov map [19, 23, 24] which equation is:

$$x_{n+1} = f(x_n, y_n) = \frac{\alpha}{1 + x_n^2} + y_n \ , \tag{2a}$$

$$y_{n+1} = g(x_n, y_n) = y_n - \beta x_n - \sigma \ . \tag{2b}$$

The Rulkov map mimics the behavior of complex continuous time neuronal models [19, 23, 24]. These equations display a variety of dynamics depending on the control parameters

α and σ. The two tipical regimes are the spiking regime: a succession of sustained pulses appears which reminds the spike train of a neuron; and the bursting regime: a brief train of short pulses alternates with a silent phase. An interesting point is the chaoticity of the trajectory in both regimes. The Rulkov map is not based on physiological observations on neurons, it is an abstract mathematical model. However, we could consider the variable x as the neuron membrane voltage and y as the concentration of a ion that interacts with the membrane.

The map (2) possesses only one fixed point $(x^*, y^*) = (-\sigma/\beta, -(\alpha + 2)/2)$. We fix $\beta = \sigma = 0.001$. The fixed point is stable for $0 < \alpha < 2$. The map exhibits sustained periodic pulses, chaotic bursts of pulses, sustained chaotic pulsing and periodic sequences of pulses for certain range of α values greater than 2 [19, 23, 24]. Since our goal is to analyze the VR phenomenon in the two maps, we need to drive them by the following biharmonic signal:

$$F(n) = f \cos \omega n + g \cos \Omega n \ , \quad \Omega \gg \omega \ , \tag{3}$$

where $F(n)$ is added to the right-hand sides of Eqs. (1) and (2a).

A. Resonance in the Bellows Maps

First, we analyze the map (1) for a parameter choice where the system is in a bistable regime. We fix $b = 2$, $r = 2$, $f = 0.1$, $\omega = 0.1$ and $\Omega = 1$ and treat the amplitude g of the high-frequency signal as the control parameter. Since we are dealing with a discrete-time system, the maximal frequency we can apply is $\Omega = \pi$. There are two coexisting attractors, one around the fixed point x_+^* and another one around x_-^* when $g = 0$. Furthermore, there is no cross-motion between the two attractors for this value of f. We iterate the map with an initial value x_0 and leave the first 10^4 iterations as a transient. To identify the various frequencies present in the solution, the power spectrum is computed using the fast Fourier transform technique. Figure 1 shows the amplitude A of the various frequency components which are present in the solution for three values of g. The dominant peaks occur only at the two frequencies $\omega = 0.1$ and $\Omega = 1$. That is, the solution essentially contains a slow motion with the frequency ω and a fast motion with the frequency Ω. The amplitude A corresponding to the frequency Ω increases with g. The amplitude at the frequency ω increases and then decreases as g is varied, which is an indication of the occurrence of VR:

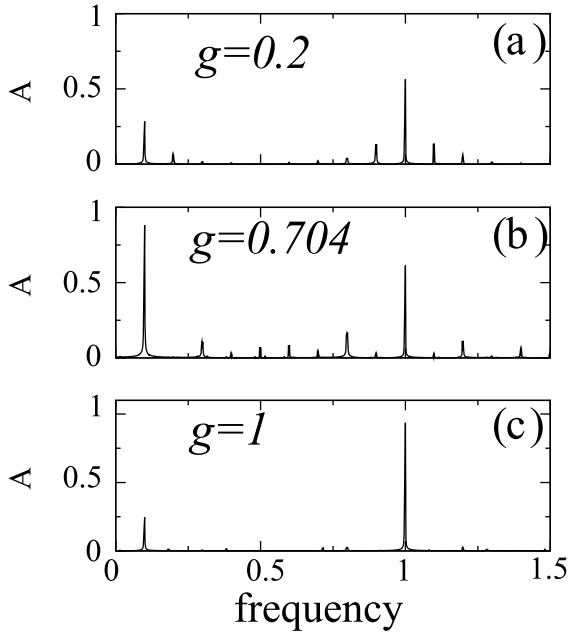

FIG. 1: Amplitude of the various frequency components of the solution of the Bellows map driven by the biharmonic signal $F(n) = f\cos\omega n + g\cos\Omega n, \quad \Omega \gg \omega$, for three values of g. The rest of the parameters fixed at $b = 2$, $r = 2$, $f = 0.1$, $\omega = 0.1$ and $\Omega = 1$. The spectrum has dominant peaks only at the frequencies ω and Ω.

the low-frequency ω is enhanced by the high-frequency signal.

We focus our analysis on the low-frequency component of the output signal which exhibits resonance. We compute the response amplitude $Q = A/f = \sqrt{Q_{\rm S}^2 + Q_{\rm C}^2}/f$ at the low-frequency only where

$$Q_{\rm S} = \frac{2}{NT}\sum_{n=1}^{NT} x_n \sin\,\omega n\ , \tag{4a}$$

$$Q_{\rm C} = \frac{2}{NT}\sum_{n=1}^{NT} x_n \cos\,\omega n\ , \tag{4b}$$

where $T = 2\pi/\omega$ and N is very large. The numerical values of $Q_{\rm S}$ and $Q_{\rm C}$ are related to the Fourier spectrum of the time series x computed at the frequency ω. In the numerical calculation of Q, N is chosen as 10^3. Figure 2(a) shows the variation of Q with g for four values of r. There is no resonance for $r \leq 1$ and in this case Q decreases monotonically with g. We note that for $r \leq 1$ the map has only one fixed point at $x^* = 0$. In Fig. 2(a), for $r = 1.5$ and 2 as g increases Q increases, reaches a maximum value at $g = g_{\rm VR} = 0.4$ and

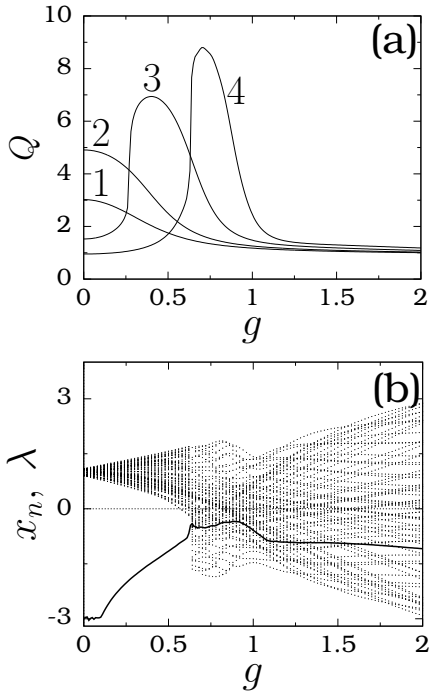

FIG. 2: (a) Response amplitude Q versus the control parameter g for four values of r in the Bellows map. The values of r for the curves 1, 2, 3 and 4 are 0.75, 1, 1.5 and 2 respectively. (b) x_n versus g (represented by dots) and the variation of Lyapunov exponent (thick curve) for $r = 2$.

0.704 respectively and then decays to zero. The vibrational resonance phenomenon occurs only for parameter values $r > 1$. Both $g_{\rm VR}$ and $Q_{\rm max}$ (the value of Q at $g_{\rm VR}$) increase with growing values of r. It is worth to notice that in this case the system is bistable so that the system switch from one state to another.

In Fig. 2(b) we plotted x_n and the Lyapunov exponent λ of the trajectory versus g for $r = 2$. The Lyapunov exponent is given by

$$\lambda = \lim_{N\to\infty} \frac{1}{NT} \sum_{n=1}^{NT} \ln |f'(x_n)|. \tag{5}$$

We can observe from this figure that the Lyapunov exponent λ is negative for the entire range of values of g implying that the time series of the map is periodic. For $g < 0.623$ the iterated values of the map stay around the fixed point $x_+^* = \sqrt{r-1}$. The attractor confined around $x_-^* = -\sqrt{r-1}$ can be obtained for certain initial values x_0. At $g = 0.623$, the onset of the jumping motion between the two fixed points $x_\pm^*$ takes place. However, resonance does not occur at this value of g, but it does at the slihgtly higher value $g = 0.704$.

In order to capture the mechanism of the resonance, we use the time series plot. Figure 3 illustrates the nature of x_n for four values of g and $r = 2$:

- For $g = 0.0$ in Fig. 3(a) there are two coexisting oscillatory solutions: one in the neighbourhood of x^*_+ and another one near x^*_-.

- When $g \neq 0$ and small, again two oscillatory solutions occur. However, these solutions are modulated by the high-frequency signal $g \cos \Omega n$. This type of solution exists for values $g < 0.623$. For $g = 0.627$ in Fig. 3(b), x_n switches between the regions $x < 0$ and $x > 0$ around the two fixed points $x^*_\pm$ and the residence times of the trajectories in these two regions are different.

- At $g = 0.704$, in Fig. 3(c), we can clearly notice periodic switching between the two fixed points and at this value of g the response amplitude Q becomes maximal.

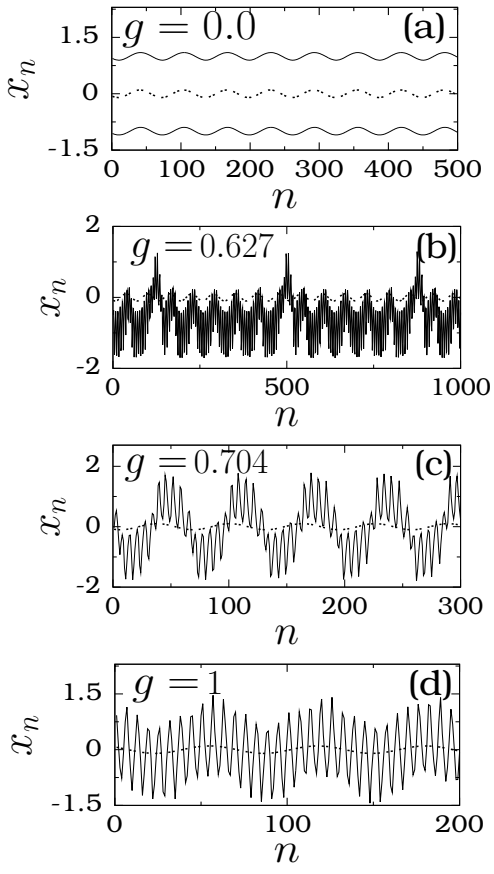

FIG. 3: x_n versus n (continuous curve) for a few values of g for the Bellows map. The dashed curve represents the periodic signal $f \cos \omega n$. Resonance occurs at $g = 0.704$.

Whenever the periodic signal $f\cos\omega n$ becomes maximal, x_n crosses from the region $x < 0$ to $x > 0$. Crossing of x_n from $x > 0$ to $x < 0$ takes place when the input signal $f\cos\omega n$ becomes minimal. The mean residence times in $x < 0$ and $x > 0$ regions are $T/2$ where $T = 2\pi/\omega$.

- When g is increased further from $g = g_{\rm VR}$, the mean residence times in $x < 0$ and $x > 0$ regions decrease and a rapid switching between these regions occur. An example is given in Fig. 3(d).

B. Resonance in the Rulkov Map

Experimental evidences in neurons has shown that an unwanted source of noise can enhance the detection of a sub-threshold input signal [19]. This parasitic signal can be a fast varying sinusoidal pertubation which improves the response of the neuron to the slow periodic input, which is the very mechanism of the VR. Here we illustrate this phenomenon using the Rulkov map in Eq. (2). We have chosen the values of the parameters as $\beta = \sigma = 0.001$, $\alpha = 1.99$. When the system is driven only by the low-frequency signal, the iterations remain near the fixed point for sufficiently small values of the amplitude f. For amplitudes above a critical value $f_{\rm c}$, pulse solutions occur where the system spends a certain amount of time near the fixed point, and then they exhibit a large excursion before returning to the neighbourhood of the fixed point in a pulse-like form. The input signal is said to be subthreshold if $f < f_{\rm c}$ [24] since it does not triggers any excursion in the phase space. In the Rulkov map, the value of $f_{\rm c}$ is found to be 0.006 for $\omega = 0.1$.

We now proceed to study VR in the Rulkov map driven by both a low-frequency and a high-frequency signal. We have chosen $f = 0.005$, a parameter value less than the sub-threshold value $f_{\rm c}$ with oscillatory motion and $f = 0.06$, a value higher than $f_{\rm c}$ with a pulse solution. Figure 4 presents Q versus g for $f = 0.005$ with $\Omega = 0.5$ and $f = 0.06$ with $\Omega = 1$. The resonance is observed for both values of f when g is varied. For $f = 0.005$ and 0.06 the response amplitude Q is maximal at $g = g_{\rm VR} = 0.23$ and $g = g_{\rm VR} = 0.44$ respectively. **The obtained bell-shaped curve is a clear indicator of an amplification of the low frequency signal by the system, as the one obtained in biological neurons in**

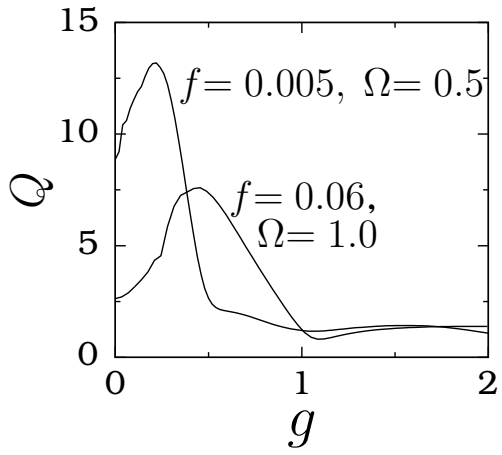

FIG. 4: Variation of the response amplitude Q as a function of the control parameter g in the Rulkov map driven by the biharmonic signal $F(n)$ for two sets of values of f and Ω. The values of the other parameters are $\beta = \sigma = 0.001$ and $\omega = 0.1$.

the stochastic resonance phenomena.

Figure 5 displays x_n versus n for a few values of g and for $f = 0.005$. For almost any value of g, x_n oscillates around the fixed point without any pulse-like motion. The high-frequency signal induces a resonance in the sense that the motion of x_n is amplified. In this connection, we wish to point out that such type of VR has been already reported in a monostable quintic oscillator [10], an asymmetric Duffing oscillator [25] and a Duffing oscillator with time-delayed feedback [16].

Following our exploration, we consider the choice $f = 0.06 > f_c$. In Fig. 6 we have plotted x_n versus n for four different values of g. By comparing the Fig. 6 with the Figs. 3 and 5, we can notice the differences and similarities between the resonance dynamics of the Bellows map (bistable case) and the Rulkov map (excitable case and also the pulse solution case) driven by the biharmonic signal. In the Rulkov map, as shown in Figs. 6(a) for $g = 0$ and also for small values of g, x_n oscillates around the fixed point and occasionally moves away from its neighbourhood. This means that the pulse-like profile of the solution persists. In the Bellows map, for small values of g, two oscillatory solutions exist around the two fixed points, as shown in Fig. 3(a). However, as g increases, the modulation of x_n by the high-frequency signal grows and the shape of the trajectory profile changes from a rectangular pulse to a sinusoidal. At $g = 0.44$, where Q becomes maximal, the trajectory

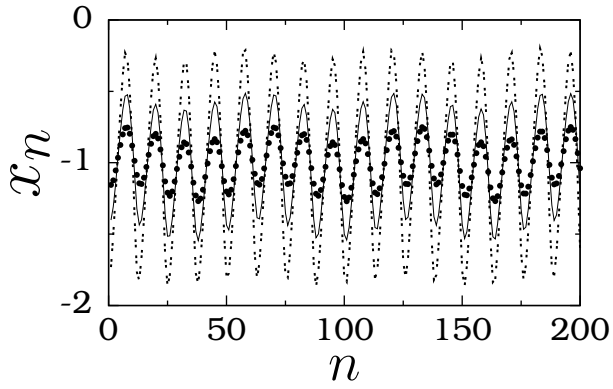

FIG. 5: Plot of x_n versus n for the Rulkov map at three values of g and with $f = 0.005$, $\omega = 0.1$ and $\Omega = 0.5$. The values of g for the dotted curve (inner most curve), continuous line curve (middle curve) and the dashed curve (outer most curve) are 0.1, 0.23 and 0.4 respectively. The resonance occurs at $g = 0.23$.

evolves into an amplitude modulated sinusoidal pattern. This is clearly seen in Fig. 6(c). Furthermore, we notice a synchronization between x_n and $f\cos\omega n$. The time duration between two consecutive returns to the neighbourhood of the fixed point is $\approx T(= 2\pi/\omega)$. This time duration decreases with a further increase in g and for the values of g far after resonance, and a rapid oscillation occurs as shown in Fig. 6(d). Compared to the case of $f = 0.005$ ($f < f_c$) for $f = 0.06$ ($f > f_c$), we can clearly notice a signature of resonance on x_n.

III. RESONANCE AND SIGNAL PROPAGATION IN m-COUPLED MAPS

Very recently, the possibility of signal propagation has been investigated in one-way coupled [26], in globally coupled [27] and in multilayer feedforward network based on the FitzHugh–Nagumo model [28]. In this section we explore the features of the propagation of the low-frequency signal in m unidirectionally coupled Bellows maps and Rulkov maps with the biharmonic signal applied to the first map only.

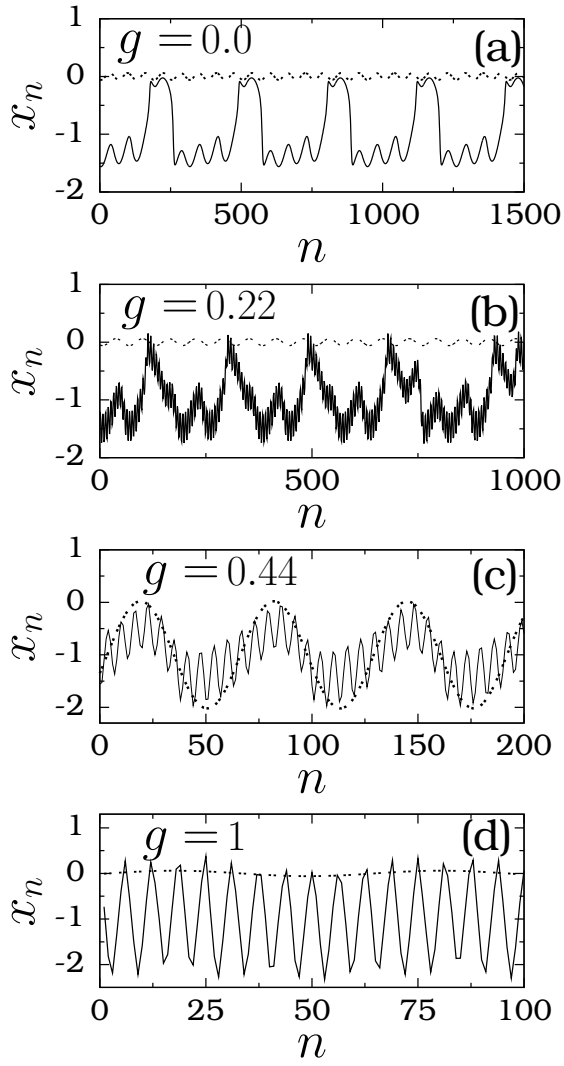

FIG. 6: Plot of x_n versus n for the Rulkov map at four values of g with $f = 0.06$, $\omega = 0.1$ and $\Omega = 1$. The continuous and dashed curves represent x_n and the low-frequency signal $f \cos \omega n$ respectively. Resonance occurs at $g = 0.44$. In the subplot (c) the amplitude and the phase of the low-frequency signal is rescaled in order to show the synchronized motion between x_n and the input signal $f \cos \omega n$.

A. Features of Undamped Signal Propagation in m-Coupled Bellows Maps

The mathematical expression of the m unidirectionally coupled Bellows maps is given by

$$x_{n+1}^{(1)} = \frac{r x_n^{(1)}}{1 + \left(x_n^{(1)}\right)^b} + f \cos \omega n + g \cos \Omega n \ , \tag{6a}$$

$$x_{n+1}^{(i)} = \frac{r x_n^{(i)}}{1 + \left(x_n^{(i)}\right)^b} + \delta x_n^{(i-1)} \ , \quad i = 2, 3, \cdots, m. \tag{6b}$$

In our analysis, we have made the choice of parameters $b = 2$, $r = 2$, $f = 0.1$, $\omega = 0.1$, $\Omega = 1$ and $m = 100$. First, in the (δ, g) parameter space we identify the regions where an undamped propagation of the signal with a component at frequency ω is possible. We divide the (δ, g) parameter space in the interval $\delta \in [0, 1]$ and $g \in [0, 15]$ into a number of grid points with $\Delta g = 0.01$ and $\Delta\delta = 0.01$. We denote Q_i as the response amplitude of the ith system in Eq. (6) at the frequency ω of the low-frequency signal. For each grid point, we calculate Q_i for all the maps. $Q_{100}(g, \omega) > Q_1(g, \omega)$ is used as a criterion for undamped and enhanced signal propagation in the coupled systems.

In Fig. 7, the black regions correspond to an enhanced signal propagation and in the white regions Q_i decays to zero as i (the number of the system) increases. For $\delta < \delta_c = 0.32$, Q_i decays with i for all values of g, that is, the signal is damped out when it propagates through the chain of oscillators. As δ increases, the width of the intervals of g where undamped signal propagation takes place increases. Figure 7 has a very close resemblance with that reported by Yao and Zhan [26] for the one-way coupled overdamped bistable oscillators. In the undamped regions for fixed values of g and δ, the value of Q_i increases with the number i and becomes a constant with $Q_{100} > Q_1$ for $i \gg 1$. In the damped regions a decay to zero happens for simillar parameters. The variation of Q_i with i has a sigmoidal shape. This is shown in Fig. 8 for few values of g for $\delta = 0.55$.

In Fig. 9 we plotted x_n versus n for $i = 2$, 3 and 8 for $\delta = 0.55$ and $g = 0.73$. This figure presents another interesting result. For fixed values of the parameters, the amplitude of the high-frequency component decreases when the number of the system i increases. This is clearly evident in Fig. 9. For large i the amplitude modulation with the frequency Ω on the output signal due to the applied high-frequency signal in the first map in Eqs. (6) almost disappears. This is further verified by numerically computing $Q_i(\Omega)$, which is found

to decay when i increases. Interestingly, for a large value of i the output signal appears as a rectangular pulse, consisting of the frequency ω and their first harmonics. This characteristic property of the coupled systems driven by a biharmonic signal in the VR setup can be used for propagating a weak signal to distant systems. It is noteworthy to point out that in the coupled system, the weak low-frequency and the high-frequency signals are applied to the first map only. The coupling of the maps essentially weakens the propagation of high-frequency components acting as a low-pass filter.

B. Multiple Resonances and their Characteristics

In Fig. 7 we notice several branches of black regions. One resonance peak (which can be sharp or wide) occurs at least in a branch in each of the coupled maps, for a fixed value of δ when g is varied. (The first map is uncoupled and shows only one resonance.) For example, for $\delta = 0.35$ and 0.4, there are two and four intervals respectively of g where $Q_{100} > Q_1$. Figure 10 displays Q versus g and i for four values of the coupling constant δ. We can clearly see two and four resonances in each coupled system for $\delta = 0.35$ and 0.4 respectively. For $\delta = 1$, Fig. 7 has only one interval $[0.63, 15]$, where an undamped propagation of the signal occurs and in Fig. 10 we observe only one resonance. As δ increases from $\delta_c = 0.32$, the spacing between successive $g_{\rm VR}$ (at which resonance occurs) decreases.

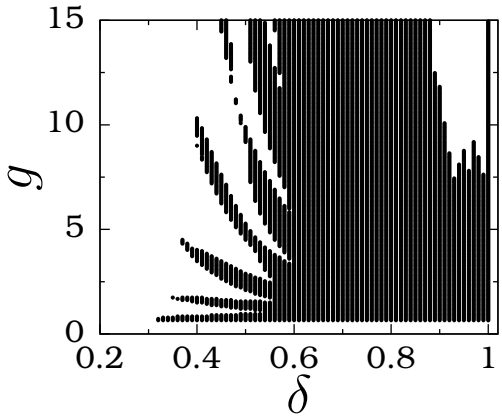

FIG. 7: Undamped signal propagation regions represented by black colour in the (δ, g) parameter space for the coupled Bellows maps. The values of the other parameters in Eqs. (6) are $b = 2$, $r = 2$, $f = 0.1$, $\omega = 0.1$, $\Omega = 1$ and $m = 100$.

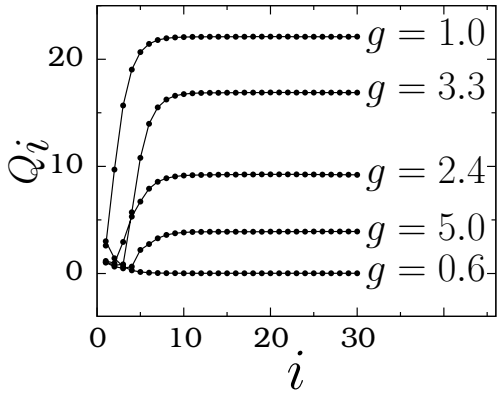

FIG. 8: Sigmoid function type variation of Q_i with i for $\delta = 0.55$ and a few fixed values of g in the coupled Bellows maps. For $g = 0.6$ a damped signal propagation takes place. For other values of g, an undamped signal propagation is realized.

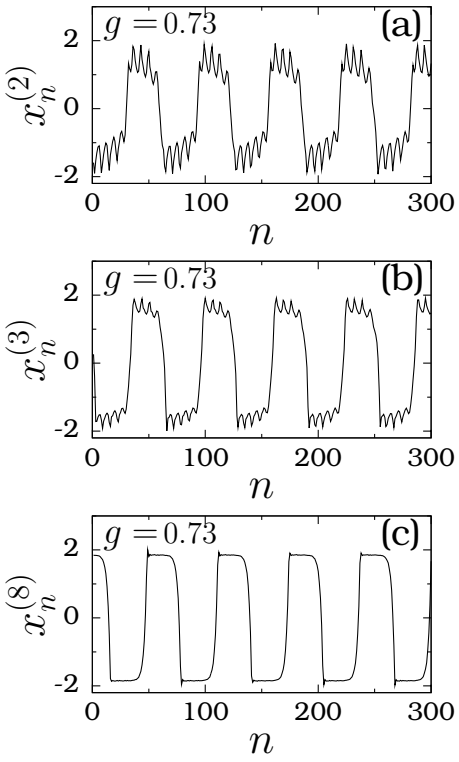

FIG. 9: Evolution of the trajectory profile from an amplitude modulated pulse form into a rectangular pulse form with an increase in the number of the system i in the coupled Bellows maps with $\delta = 0.55$ and $g = 0.73$.

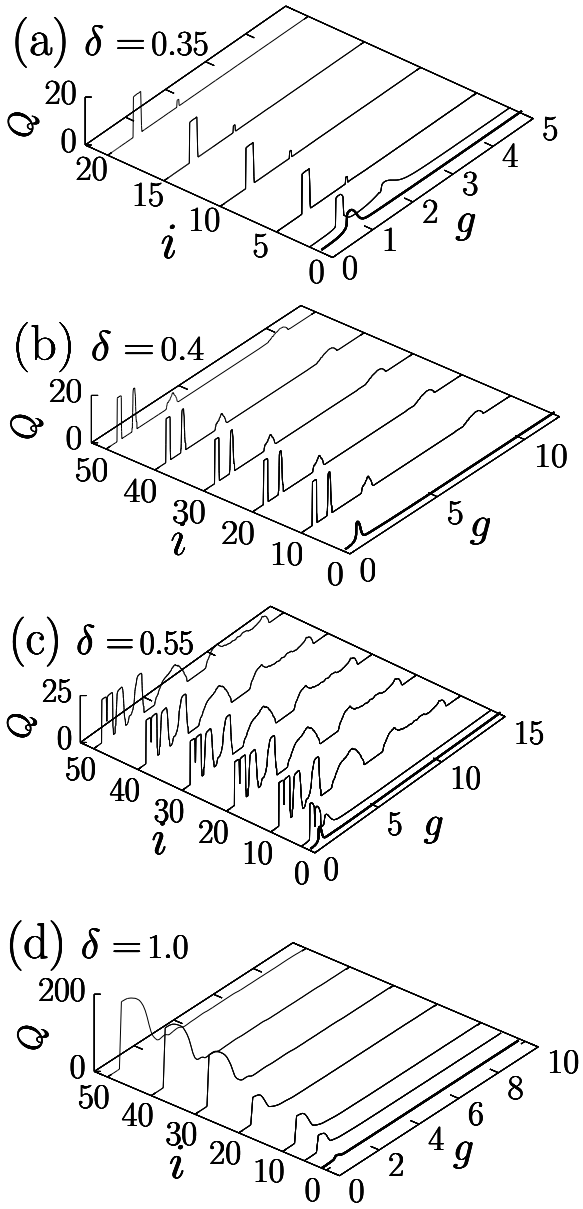

FIG. 10: Q versus g and i for the coupled Bellows maps for a few values of δ. The effect of the coupling constant can be clearly seen. Initial resonance peaks are wide.

We notice four resonances when g is varied in Fig. 10(b) for $\delta = 0.4$. However, the value of the response amplitude Q at successives resonances is reduced considerably. To take this fact into account, we have computed the mean residence time of the iterations in the regions $x < 0$ and $x > 0$. A residence time in the region $x < 0$ is the difference between the time at which x_n enters the region $x < 0$ and leaves this region and enters into the region $x > 0$. Similarly, we can define a residence time of x_n in the region $x > 0$. We denote τ_+ and τ_- as

mean residence times in the regions $x > 0$ and $x < 0$ respectively and $\tau = \tau_+ + \tau_-$. We have numerically computed 10^5 residence times in $x < 0$ and $x > 0$ for the 25th ($i = 25$) system of Eqs. (6), for the parameter value $\delta = 0.4$ and for a range of values of g. After that, we have computed τ_+, τ_- and τ.

Figure 11 presents the variation of Q and τ around the four resonances.

- In Fig. 11(a), Q is maximal with a plateau over a wide range of g. In this interval of g, τ_+ and τ_- vary in such a way that $\tau = \tau_+ + \tau_- \approx T = (2\pi/\omega)$.

- The second resonance region in Fig. 11(b) is similar in shape to Fig. 11(a). $Q_{\max}$ has almost the same value and $\tau \approx T$.

- Next, in Fig. 11(c) at the resonance occurring at $g = 3.85$ $\tau = 186.64 \approx 3T$.

- At the fourth resonance shown in Fig. 11(d), we have found that $\tau \approx 375.86 \approx 6T$. It is noteworthy to point out that in Fig. 11 τ is locally minimal at all the resonances. When $\tau \approx T$, there is a periodic switching between the regions $x < 0$ and $x > 0$. This is shown in Fig. 12 for $g = 0.7$ and 1.6. When $\tau \approx lT$ with $l > 1$, there is no periodic switching between the two regions (see Fig. 11(c) and (d)), however, a resonance occurs. At this resonance the value of Q is relatively much smaller than the value of Q at other resonances with $\tau \approx T$.

C. m-Coupled Rulkov Maps

We consider m-coupled unidirectionally Rulkov maps

$$x_{n+1}^{(1)} = f\left(x_n^{(1)}, y_n^{(1)}\right) + f\cos\,\omega n + g\cos\,\Omega n\,, \tag{7a}$$

$$x_{n+1}^{(i)} = f\left(x_n^{(i)}, y_n^{(i)}\right) + \delta x_n^{(i-1)}\,, \quad i = 2, 3, \cdots, m \tag{7b}$$

$$y_{n+1}^{(i)} = g\left(x_n^{(i)}, y_n^{(i)}\right)\,, \quad i = 1, 2, \cdots, m \tag{7c}$$

$$\tag{7d}$$

where $f(.)$ and $g(.)$ are given in Eq. (2). Very recently, Wang and Chen [29] investigated delay-induced intermittent synchronization in coupled Rulkov maps. Here we fix parameters to be $\beta = \sigma = 0.001$, $f = 0.06$, $\omega = 0.1$, $\Omega = 1$ and $m = 100$.

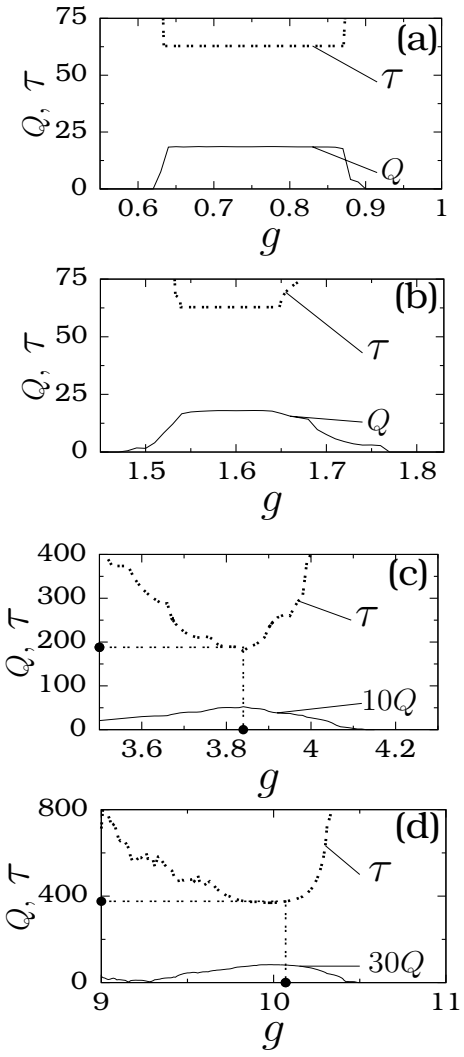

FIG. 11: Variation of $\tau = \tau_+ + \tau_-$ near four resonances in the 25th system of the coupled Bellows maps with $\delta = 0.4$. The variation of Q is also shown for identifying the connection between resonance and τ. In the subplots (c) and (d), Q is rescaled by a factor for clarity.

Figure 13 shows the parametric values of δ and g for which an undamped signal propagation takes place. For $\delta < 0.18$ a damped propagation occurs for any value of g. Similar to the coupled Bellows maps, in the regions of undamped signal propagation at a given g and δ, the response amplitude Q_i of the ith map increases when i increases and then saturates to a constant value. This is clearly seen in Fig. 14 for $\delta = 0.3$ and 0.5. For $\delta = 0.5$, a multiple resonance with wide resonance interval of g and sharp peaks occurs for $i \gg 1$. Figure 15 shows $x_n^{(50)}$ versus n at $g = 0.5$ and 6.8, where a resonance is found with $Q_{\max} = 29.8$ and

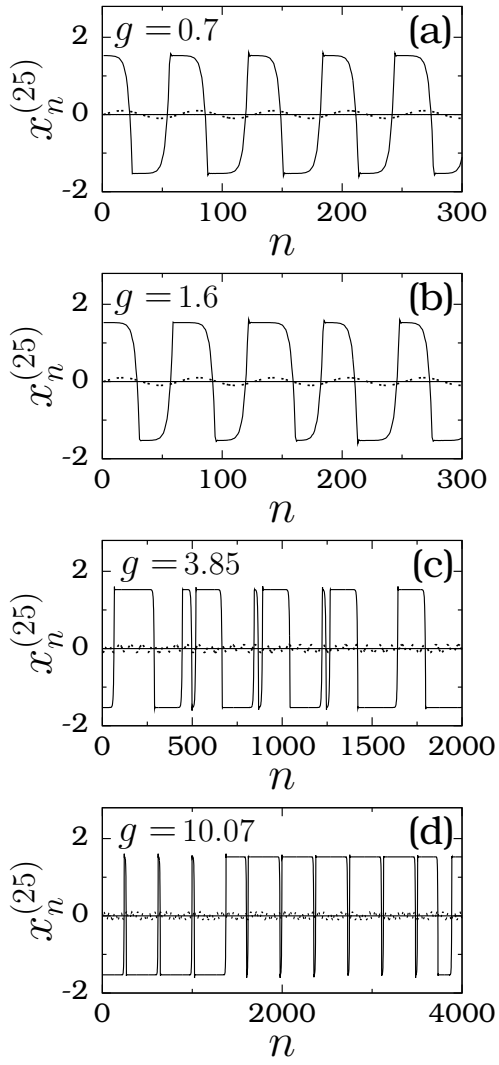

FIG. 12: Iteration plot at four resonances of the 25th system of the coupled Bellows maps with $\delta = 0.4$.

20.5 respectively. In the vicinity of the fixed point, x_n varies linearly with a slow rate, while in the excursion region it oscillates rapidly.

We have computed the mean residence times of $x_n^{(50)}$ in the vicinity of the fixed point (τ_-) and in the oscillatory region (τ_+) and $\tau = \tau_+ + \tau_-$ for a range of values of g with $\delta = 0.5$. The result is presented in Fig. 16. In the first two resonances, where Q is maximal for wide intervals of g, the value of $\tau \approx T = 62.83$. At other resonance values of g also $\tau \approx T$.

IV. CONCLUSION

In the present work, we report our investigation on the phenomenon of VR in two different types of maps, the Bellows and the Rulkov map. In both maps, resonance at the low-frequency ω is induced by the high-frequency signal. Some common and different features are observed in these two maps. At resonance, in the Bellows map, a periodic switching between the two coexisting states occurs. In the Rulkov map we have two distinct cases. For $f < f_c$, when $g = 0$ an oscillatory motion around the only fixed point takes place. When g is varied resonance occurs, however, there is no switching between any two kinds of states and the oscillatory motion persists. For $f > f_c$, when $g = 0$ a pulse solution occurs. In this case, as g is varied at the resonance, the pulse solution becomes an amplitude modulated sinusoidal waveform.

In the coupled maps, for a range of coupling strength and the amplitude of the high-frequency signal, an undamped propagation of signal appears, even though the first map alone is driven by the biharmonic signal. We note that by maintaining the undamped signal propagation, the response amplitude Q can be controlled by suitably choosing the values of δ and g. Another interesting result is the occurrence of multiple resonances in the coupled maps i. Furthermore, each resonance occurs at the same value of g in the coupled maps and the response amplitude profile reaches a stationary pattern as the system number i

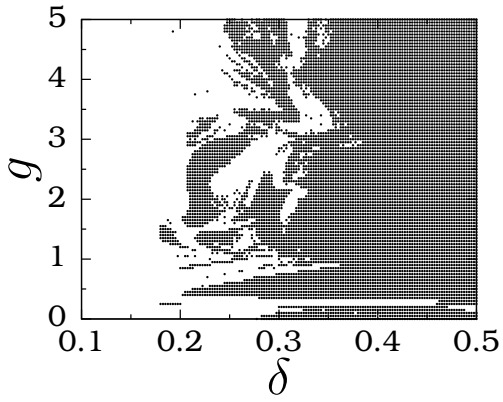

FIG. 13: Regions of undamped signal propagation in the (δ, g) parameter space represented by black colour for the coupled Rulkov maps. The values of the other parameters in Eqs. (7) are $\beta = \sigma = 0.001$, $f = 0.06$, $\omega = 0.1$, $\Omega = 1$ and $m = 100$.

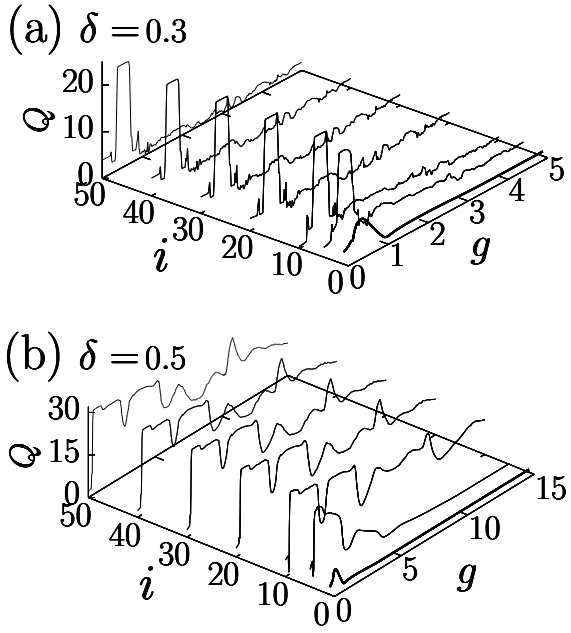

FIG. 14: Response amplitude Q versus g and i for the coupled Rulkov maps for two values of the coupling constant δ.

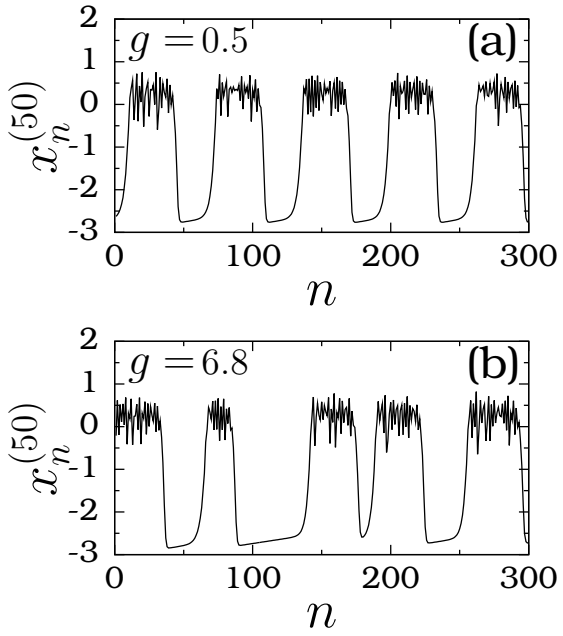

FIG. 15: Plot $x_n^{(50)}$ versus n for the coupled Rulkov maps with $\delta = 0.5$ and for two values of g at which resonance occurs.

increases. In the coupled Bellows maps at resonance, the sum of the mean residence times τ

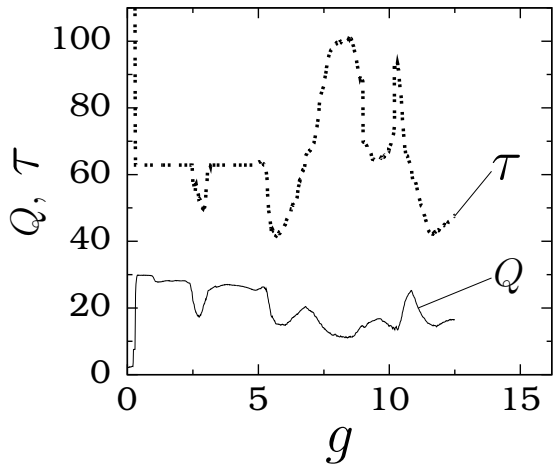

FIG. 16: Variation of the response amplitude Q and $\tau = \tau_+ + \tau_-$ of 50th system of the coupled Rulkov maps for a range of values of g with $\delta = 0.5$.

is a multiple of T, where T is the period of the low-frequency force. In the coupled Rulkov maps with $f > f_c$ at resonance, we get $\tau \approx T$.

Simple discrete maps not only exhibit complex dynamics, but they are also useful for the study of general nonlinear phenomena. We believe that the results reported on the two maps will lead to a detailed analysis of others types of resonances such as stochastic, coherence and auto-resonances in maps resulting in further understanding of these resonances and their applications.

Acknowledgments

Financial support from the Spanish Ministry of Science and Innovation under Project No. FIS2009-09898 is acknowledged.

---

[1] L. Gammaitoni, P. Hanggi, P. Jung, and F. Marchesoni, Rev. Mod. Phys. **70**, 223 (1998).

[2] M.D. McDonnell, N.G. Stocks, C.E.M. Pearce, and D. Abbott, *Stochastic resonance: From suprathreshold stochastic resonance to stochastic signal quantization* (Cambridge University Press, Cambridge, 2008).

[3] P.S. Landa and P.V.E. McClintock, J. Phys. A: Math. Gen. **33**, L433 (2000).

[4] M. Gitterman, J. Phys. A: Math. Gen. **34**, L355 (2001).

[5] I.I. Blekhman and P.S. Landa, Int. J. Nonlin. Mech. **39**, 421 (2004).

[6] A.A. Zaikin, L. Lopez, J.P. Baltanas, J. Kurths, and M.A.F. Sanjuan, Phys. Rev. E **66**, 011106 (2002).

[7] E. Ullner, A. Zaikin, J. Garcia-Ojalvo, R. Bascones, and J. Kurths, Phys. Lett. A **312**, 348 (2003).

[8] V.M. Gandhimathi, S. Rajasekar, and J. Kurths, Phys. Lett. A **360**, 279 (2006).

[9] S. Jayakumari, V. Chinnathambi, S. Rajasekar, and M.A.F. Sanjaun, Chaos **19**, 043128 (2009).

[10] S. Jayakumari, V. Chinnathambi, S. Rajasekar, and M.A.F. Sanjaun, Phys. Rev. E **80**, 046608 (2009).

[11] B. Deng, J. Wang, and X. Wei, Chaos **19**, 013117 (2009).

[12] B. Deng, J. Wang, X. Wei, K.M. Tsang, and W.L. Chan, Chaos **20**, 013113 (2010).

[13] S. Rajasekar, K. Abirami and M.A.F. Sanjuan, Chaos **21**, 033106 (2011).

[14] J.H. Yang and X.B. Liu, J.Phys. A: Math. Theor. (2011, in press).

[15] J.H. Yang and X.B. Liu, J.Phys. A: Math. Theor. **43**, 122001 (2010).

[16] C. Jeevarathinam, S. Rajasekar, and M.A.F. Sanjuan, Phys. Rev. E **83**, 066205 (2011).

[17] K. Kaneko and I. Tsuda, *Complex systems: Chaos and beyond "A constructive approach with applications in life sciences"* (Springer, Berlin, 2001).

[18] H.G. Schuster and W. Just, *Deterministic chaos: An introduction* (Wiley-VCH, Weinheim, 2005).

[19] B. Ibarz, J.M. Casado, and M.A.F. Sanjuan, Phys. Rep. **501**, 1 (2011).

[20] T.S. Bellows, J. Anim. Ecol. **50**, 139 (1981).

[21] K. Masutani, Bull. Math. Biol. **55**, 1 (1993).

[22] S. Sinha and P.K. Das, Pramana J. Phys. **48**, 87 (1997).

[23] N.F. Rulkov, Phys. Rev. Lett. **86**, 183(2001).

[24] R.C. Hilborn, Am. J. Phys. **72**, 528 (2004).

[25] S. Jayakumari, V. Chinnathambi, S. Rajasekar, and M.A.F. Sanjuan, Int. J. Bifur. & Chaos **21**, 275 (2011).

[26] C. Yao and M. Zhan, Phys. Rev. E **81**, 061129 (2010).

[27] J.H. Yang and X.B. Liu, Phys. Scr. **83**, 065008 (2011).

[28] Y. Qin, J. Wang, C. Men, B. Deng, and X. Wei, Chaos **21**, 023133 (2011).

[29] Q. Wang and G. Chen, Chaos **21**, 013123 (2011).